JOURNAL OF GEOPHYSICAL RESEARCH: SPACE PHYSICS, VOL. 118, 4161–4175, doi:10.1002/jgra.50394, 2013

Primary and secondary compressible Kelvin-Helmholtz surface wave instabilities on the Earth's magnetopause

H. Turkakin,[1] R. Rankin,[1] and I. R. Mann[1]

Received 14 February 2013; revised 4 June 2013; accepted 8 June 2013; published 12 July 2013.

[1] Primary and secondary Kelvin-Helmholtz surface wave modes on the Earth's magnetopause are studied within the framework of warm plasma ideal magnetohydrodynamics (MHD) across an infinitely thin magnetopause tangential discontinuity (TD). With the increase of background flow velocity, a Kelvin-Helmholtz Instability (KHI) unstable boundary separating two uniform semi-infinite plasma regions is always ultimately stabilized to KHI growth at an upper cut-off while inclusion of an inner boundary in one plasma region removes this stabilization. Phase velocity Friedrichs diagrams are presented that allow us to identify unstable fast and slow modes that correspond to growing modes of the KHI under different magnetosphere and magnetosheath conditions. On the nightside magnetosphere, and the magnetotail, new KH unstable intermediate-fast modes are created, which cannot propagate exactly perpendicular to the magnetic field. In the plasma frame, primary unstable KH waves show fast/fast, while secondary KH waves show slow/fast mode behavior in the magnetosphere/magnetosheath. Secondary KHI occurs at slower flow speeds than the primary KHI and grows more slowly and at a narrow range of propagation angles. Our analysis is placed in the context of in situ satellite observations of the phase speed of KHI-related waves in the magnetosheath and magnetosphere in the long wavelength regime where our analysis applies. We conclude that KH unstable surface waves on the near-Earth magnetopause flanks are likely to be secondary KHI waves, while those further down the flanks and on the nightside magnetopause are likely to be primary KHI waves—the latter being the most important for energy transport at the magnetopause.

Citation: Turkakin, H., R. Rankin, and I. R. Mann (2013), Primary and secondary compressible Kelvin-Helmholtz surface wave instabilities on the Earth's magnetopause, *J. Geophys. Res. Space Physics*, *118*, 4161–4175, doi:10.1002/jgra.50394.

1. Introduction

[2] The Kelvin-Helmholtz Instability (KHI) can arise when the equilibrium of a stratified heterogeneous fluid with relative motion in different layers is considered [*Chandrasekhar*, 1961]. It evolves temporally and/or spatially corresponding to whether wave modes grow with time and space, respectively [e.g., *Itoh et al.*, 2004]. The velocity shear between the magnetospheric and magnetosheath plasma in the Earth's magnetosphere generates a magnetohydrodynamic KHI, which plays an important role in many magnetospheric phenomena, such as the generation of geomagnetic pulsations [*Southwood*, 1974; *Walker*, 1981; *Miura and Pritchett*, 1982; *Chen and Hasegawa*, 1993; *Rae et al.*, 2005; *Villante*, 2007; *Agapitov et al.*, 2009], magnetic reconnection and plasma mixing at the magnetopause especially during northward Interplanetary Magnetic Field (IMF) [*Otto and Fairfield*, 2000; *Fairfield et al.*, 2000; *Nakamura et al.*, 2006; *Pegoraro et al.*, 2008; *Nakai and Ueno*, 2011], and as an agent for momentum and energy transfer across the magnetopause [*Pu and Kivelson*, 1983b; *Miura*, 1984; *Kivelson and Chen*, 1995; *Hasegawa et al.*, 2006]. It has also been proposed that the surface waves generated by the KHI may have an influence on substorm expansion phase onset in the plasma sheet [e.g., *Rostoker and Eastman*, 1987; *Yoon et al.*, 1996; *Lui*, 2004; *Uberoi*, 2006]. All of these are key elements for solar wind interactions with the Earth's magnetosphere and ionosphere. In the solar atmosphere, KHI is also a process that can lead to plume/interplume mixing and may be a source for Alfvénic fluctuations in the solar wind [e.g., *Andries et al.*, 2000; *Andries and Goossens*, 2001].

[3] Due to the significant effects it has on the magnetosheath-magnetosphere boundary, understanding the KHI and the behavior of the waves related to it is an active area of research in magnetospheric physics. Several early works shed light on this subject for incompressible [*Sen*, 1963] and compressible [*Fejer*, 1964; *Sen*, 1964, 1965; *Lerche*, 1966] plasmas. *Sen* [1965] identified the regions of the dayside/nightside magnetopause and magnetotail that may be KH unstable. *Southwood* [1968] studied the

[1]Department of Physics, University of Alberta, Edmonton, Alberta, Canada.

Corresponding author: H. Turkakin, Department of Physics, 3-240 CCIS, University of Alberta, Edmonton, AB T6G 2E1, Canada. (turkakin@ualberta.ca)

2169-9380/13/10.1002/jgra.50394

magnetospheric boundary allowing different magnetic fields on both sides of the magnetopause and discovered that the maximum growth rate occurs when shear flow is perpendicular to the background magnetic field.

[4] In the KHI studies, the magnetopause boundary is often assumed to have zero thickness [*Pu and Kivelson*, 1983a, 1983b; *Mann et al.*, 1999; *Mills et al.*, 1999; *Mills and Wright*, 1999]; this assumption is valid for waves with wavelengths bigger than the thickness of the boundary layer. Under this assumption, the growth rates of the KH unstable waves increase without limit as the tangential wave number increases [*Southwood*, 1968; *Ong and Roderick*, 1972; *Mann et al.*, 1999]. Study of KHI with the finite transition thickness was first done by *Ong and Roderick* [1972] employing both incompressible and compressible flow analysis. They found that the finite thickness of the transition layer stabilizes the boundary for short wavelength perturbations. They also noted that the component of the background magnetic field parallel to the shear flow reduces the growth rate of the instability and confirmed the fact that the compressibility has a stabilizing effect as well, which was suggested earlier by *Sen* [1964]. It is also found that when a boundary finite thickness is included, growth rates have a maximum value for a finite wave number and tends toward to zero growth as the wave number tends to infinity [*Ong and Roderick*, 1972; *Walker*, 1981; *Miura and Pritchett*, 1982; *Allan and Wright*, 1997].

[5] Although the KHI of the magnetopause has been investigated extensively in the past, there are still a number of features that remain to be fully explained. For instance, it is well known that there is an upper and a lower cut-off velocity for the onset of the KHI surface wave when the plasmas on both sides of the magnetopause are unbounded [*Pu and Kivelson*, 1983a, 1983b; *Mills and Wright*, 1999; *Mills et al.*, 1999; *Mann et al.*, 1999; *Taroyan and Erdélyi*, 2002, 2003a, 2003b]. It is also known that the upper cut-off velocity is removed when an inner boundary is included in the magnetosphere [*Fujita et al.*, 1996; *Mann et al.*, 1999; *Mills et al.*, 1999; *Mills and Wright*, 1999]. A lower cut-off velocity below which the boundary is stable exists due to magnetic tension on the boundary [*Pu and Kivelson*, 1983a, 1983b; *Miura*, 1995; *Mann et al.*, 1999]. The upper cut off velocity is typically explained as the point where KHI generated surface waves turn into oscillatory modes and propagate into the magnetosphere and magnetosheath stabilizing the KHI [*Fujita et al.*, 1996; *Pu and Kivelson*, 1983a; *Mann et al.*, 1999; *Mills et al.*, 1999]. However, in the bounded case there can be an influence of the inner boundary on the shear flow boundary and this has not been fully examined.

[6] Less well-known is the fact that in a compressible plasma there can be two KH unstable often distinct flow speed regions, which allow for the existence of a primary as well as a less intense secondary KHI interval, depending on the ambient plasma parameters [*González and Gratton*, 1994; *González et al.*, 2002; *Taroyan and Erdélyi*, 2002, 2003a]. This secondary instability region occurs for flow speeds typically below the primary KHI and with usually smaller growth rates. Nevertheless, the secondary instability should not be ignored since it could be the only active instability under certain physical conditions [e.g., *González et al.*, 2002] and might hence be the only means of energy propagation at the boundary. We examine the generation of the primary and secondary KHI in the context of the magnetopause KHI in this paper.

[7] When waves are incident on a nonrigid boundary such as the magnetopause, they can extract energy from the boundary and be reflected back with an enhanced amplitude and energy [e.g., *McKenzie*, 1970; *Walker*, 2000]. In this case, the transmitted wave can be considered to have negative energy in order to maintain energy conservation [*Fejer*, 1963; *McKenzie*, 1970; *Mann et al.*, 1999]. However, for the more realistic scenario where wave-packets have finite length, causality suggests that the interactions can better be described by an active boundary where, instead of assigning negative energy to the transmitted waves, energy exchange between the waves and the flow is described in terms of the work done by Reynolds and Maxwell stresses at the boundary [*Walker*, 2000]. The interaction of a negative and a positive energy wave has also previously been theorized to be an initiator of the onset of the KHI [*Cairns*, 1979; *Mills et al.*, 1999; *Taroyan and Erdélyi*, 2002, 2003a], however, we revisit this conclusion here.

[8] In the current study, the behavior of MHD modes in a bounded and unbounded magnetosphere and magnetosheath separated by a shear flow across a tangential discontinuity (TD) are explored and compared. An analysis of a bounded magnetosphere is more applicable to the dayside magnetosphere and the near-Earth flank nightside magnetosphere where the plasmapause may represent an inner boundary. Further down the magnetotail, the two regions on both sides of the magnetopause can be assumed to be semi-infinite, since the average value of the diameter of the magnetotail can reach up to $\sim 50 - 60R_E$ [*Pertinec and Russell*, 1996]. In this latter case, the boundary is far away from the shear layer to the extent that any waves reflected from the distant boundary may have little or no impact on the dynamics of the magnetopause.

[9] We describe the primary and secondary KHI and their relevance to excited MHD wave modes using the physical framework of linear mode interactions. A strong correlation between the linear interactions of MHD waves and the onset and stabilization of primary and secondary KHI is revealed. Similar studies have been performed in the past, but a clear explanation of the relationship between the wave-wave interactions and the properties of the primary and secondary KHI was not provided [e.g., *Mills et al.*, 1999; *Taroyan and Erdélyi*, 2002, 2003a, 2003b]. This framework also reveals some physics of the upper cut-off. Finally, we examine the fast and slow mode characteristics of the primary and secondary KHI waves, showing that the modes can have different characteristics of slow or fast on either side of the magnetopause. We further examine the observational implications of this in the magnetospheric context.

2. KHI Dispersion Relation and Numerical Method

[10] Observations have demonstrated that the region of the magnetopause which is most susceptible to the KHI is the low latitude boundary layer in the equatorial plane on the flanks starting from the dayside flanks and extending into the magnetotail [e.g., *Hasegawa et al.*, 2004, 2006; *Foullon et al.*, 2008, 2010]. In the present study, the dayside and nightside flanks of the magnetosphere, and the magneto-

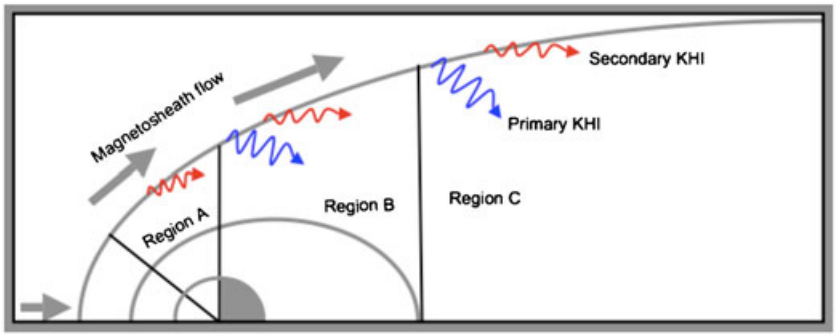

Figure 1. Regions of the magnetosphere investigated. Region A corresponds to the dayside flanks, region B corresponds to the nightside flanks, and region C corresponds to the far down the magnetotail. A representative position of the plasmapause is shown as the inner boundary for a bounded magnetosphere calculations of regions A and B. The size of the Earth is exaggerated for clarity.

tail, will all be probed along the equatorial plane for the onset of the KHI. These regions are labeled as regions A, B, and C, respectively, for clarity throughout the rest of this paper (see Figure 1). Region A corresponds to the dayside flanks of the magnetosphere, region B corresponds to the nightside flanks until distances $\simeq 10 - 15R_E$ downtail from the terminator where the plasmapause remains as a possible inner boundary, and region C is even further down the magnetotail where the shear-flow boundary is effectively unbounded on either side.

[11] In the analysis presented here, a tangential discontinuity (TD) boundary with zero thickness is assumed. At a TD, the normal components of the background magnetic field and plasma flow velocity are zero. We have assumed a zero transition thickness which is suitable if the wavelengths, λ, of the generated waves are considerably larger than the thickness, l, of the boundary. Observations have revealed that the magnetopause boundary thickness typically varies between $\sim 0.1 - 1R_E$ [e.g., *Gnavi et al.*, 2009; *Nakai and Ueno*, 2011; *Hwang et al.*, 2011], while wavelengths of long period KHI relevant waves can vary between $\sim 2 - 15R_E$ [e.g., *Chen and Kivelson*, 1993; *Kivelson and Chen*, 1995; *Owen et al.*, 2004; *Hasegawa et al.*, 2006; *Foullon et al.*, 2008; *Agapitov et al.*, 2009; *Gnavi et al.*, 2009; *Foullon et al.*, 2010; *Nakai and Ueno*, 2011; *Hwang et al.*, 2011], indicating that $\lambda \gg l$ in most cases. Therefore, a zero transition thickness can be assumed to be a valid model for the magnetopause when these long period KHI waves with long wavelengths are under investigation. Shorter period waves which will have shorter wavelengths are better explored with a model magnetopause of finite thickness [e.g., *Walker*, 1981; *Miura*, 1984; *Taroyan and Erdélyi*, 2002, 2003a, 2003b].

[12] In region A, the magnetic fields on both sides of the boundary are chosen to be perpendicular to each other. In regions B and C, the magnetic fields are set parallel (or antiparallel—the dispersion relations are symmetrical) to each other. The flow velocity is set parallel to the background magnetic field in the magnetosheath in all the regions, A, B, and C. A box model is used that corresponds to a Cartesian coordinate system with a zero transition thickness shear flow boundary, as displayed in Figure 2. In Figure 2, region 1 represents the magnetosheath, and region 2 represents the magnetosphere. $B_{01,02}$ are the background magnetic fields and d is the distance to the inner boundary in the bounded magnetosphere cases (A and B) expressed in units of the Earth's radius, R_E; d is set to ∞ for the isolated unbounded shear flow boundary in case C. $U_{01,02}$ are the background flow velocities in regions 1 and 2, where U_{01} is assumed to be directed along y and U_{02} is set to zero.

[13] The KHI is a macroscopic instability where the scale length of the generated waves is comparable to the bulk scales of the plasma [*Baumjohann and Treumann*, 2001]. Thus, an appropriate approach for studying this phenomenon is to use magnetohydrodynamics (MHD), and ideal MHD is the approach used in the current study. We follow the standard approach where the ideal MHD equations are linearized under a small amplitude approximation for compressible

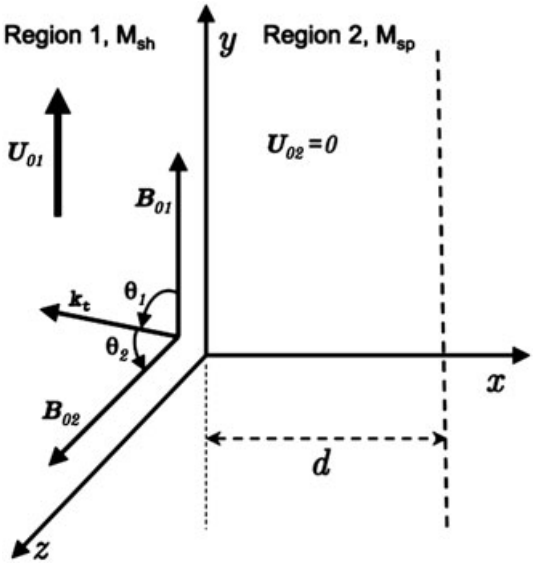

Figure 2. Model used for the bounded magnetosphere; region 1 is the magnetosheath, M_{sh}, and region 2 is the magnetosphere, M_{sp}. The magnetosheath has a uniform flow in the y direction and the magnetosphere has zero flow velocity. Both regions have background magnetic fields at arbitrary directions with respect to the direction of wave propagation. An inner boundary is set at $x = d$ in the magnetosphere for bounded magnetosphere calculations and is removed for the unbounded magnetosphere calculations.

warm homogeneous plasmas on both sides of the boundary. The dependent variables are assumed to be a superposition of an equilibrium value, g_0, and a perturbed value δg; $g(\mathbf{r}, t) = g_0(\mathbf{r}, t) + \delta g(\mathbf{r}, t)$, where g represents the dependent variable. A sinusoidal perturbation is assumed, depending on time and space as $\delta g(\mathbf{r}, t) = De^{i(\mathbf{k_t}.\mathbf{r} \pm k_x x - \omega t)}$, where ω is the complex frequency, $\mathbf{k_t}$ is the tangential wave number, $\mathbf{k_x}$ is the complex wave number normal to the boundary, and D is a constant amplitude. Perturbation along x in regions 1 and 2 is set as $e^{-ik_{x1}.x}$ and $e^{ik_{x2}.x}$, respectively [cf., e.g., *Pu and Kivelson*, 1983a]. The set up displayed in Figure 2 is used, and boundary conditions corresponding to a tangential discontinuity, namely continuity of the displacement and total pressure perturbation across the magnetopause boundary, are applied to the dispersion relation:

$$[(\omega_1')^2 - \frac{(\mathbf{B}_{01} \cdot \mathbf{k}_t)^2}{\rho_{01}\mu_0}]\frac{\rho_{01}}{k_{x1}} + [(\omega_2')^2 - \frac{(\mathbf{B}_{02} \cdot \mathbf{k}_t)^2}{\rho_{02}\mu_0}]\frac{\rho_{02}}{k_{x2}} = 0. \quad (1)$$

Here $\rho_{01,02}$ are the background mass densities and μ_0 is the permeability of free space. Rewriting equation (1) in terms of background Alfvén velocities, we obtain

$$[(\omega_1')^2 - (\mathbf{V}_{A1} \cdot \mathbf{k}_t)^2]\frac{\rho_{01}}{k_{x1}} + [(\omega_2')^2 - (\mathbf{V}_{A2} \cdot \mathbf{k}_t)^2]\frac{\rho_{02}}{k_{x2}} = 0, \quad (2)$$

where

$$\omega_{1,2}' = \omega - \mathbf{U}_{01,02} \cdot \mathbf{k}_t, \quad (3)$$

$$\mathbf{V}_{A1,A2}^2 = (\mathbf{B}_{01,02})^2/(\rho_{01,02}\mu_0), \quad (4)$$

$$k_{x1,x2}^2 = \left((\omega_{1,2}')^4 / \left[(\omega_{1,2}')^2(V_{A1,A2}^2 + C_{S1,S2}^2) - (\mathbf{V}_{A1,A2} \cdot \mathbf{k}_t)^2 C_{S1,S2}^2\right]\right) - k_t^2, \quad (5)$$

$$C_{S1,S2}^2 = \gamma P_{01,02}/\rho_{01,02}. \quad (6)$$

In equations (3)–(6), ω is the frequency in the stationary frame, $\omega_{1,2}'$ are Doppler shifted frequencies, $V_{A1,A2}$ are Alfvén velocities, $k_{x1,x2}$ are wave numbers normal to the boundary, and $C_{S1,S2}$ are the sound speeds in regions 1 and 2, respectively. The adiabatic index γ is taken as 5/3. When a perfectly reflecting boundary is included in the magnetosphere, equation (2) becomes

$$i\tan(k_{x2}d)[(\omega_1')^2 - (\mathbf{V}_{A1} \cdot \mathbf{k}_t)^2]\frac{\rho_{01}}{k_{x1}} - [(\omega_2')^2 - (\mathbf{V}_{A2} \cdot \mathbf{k}_t)^2]\frac{\rho_{02}}{k_{x2}} = 0. \quad (7)$$

[14] Eigenfrequencies of equations (2) and (7), representing an unbounded and a bounded magnetosphere, respectively, are computed numerically using a Newton-Raphson scheme. The growth rates and real frequencies of KHI unstable surface waves are determined for different sets of parameters applied to three different regions: regions A, B, and C (see Figure 1). Stable and unstable waveguide modes are also possible in the bounded magnetosphere case [*Mann et al.*, 1999], however, they are not examined in the current study. Phase velocity Friedrichs diagrams are plotted as an aid to understanding wave-wave interactions and their connection to the KHI. Group velocity diagrams are also plotted in order to investigate the direction of energy propagation of the KH unstable waves.

[15] In the following sections of the paper, normalized flow velocities $V_{01,02}$ are used such that $V_{01,02} = U_{01,02}/V_{A2}$ with normalization with respect to the Alfvén speed, V_{A2}, in the magnetosphere. The distance, d, is normalized by R_E, and wave numbers, k, are normalized by $1/d$. Normalized frequencies are, real frequencies, $\omega_r d/V_{A2}$, growth rates, $\omega_i d/V_{A2}$, and doppler shifted frequencies, $\omega_r d/V_{A2} - \mathbf{V_{01}}.\mathbf{kt}d$. The background physical parameters are set such that $\beta_1 = 2.5$, $\beta_2 = 0.64$, $B_{01}/B_{02} = 2/3$, $\rho_{01}/\rho_{02} = 10$, $k_t d = 2.82$, with V_{01} in the range of 1–10, and $V_{02} = 0$. These are characteristic values across the magnetopause [e.g., *Pu and Kivelson*, 1983a, 1983b; *Taroyan and Erdélyi*, 2003b]. Here, $\beta_{1,2} = (P_{01,02})/(B_{01,02}^2/2\mu_0)$, such that the parameters chosen represent realistic values of the plasma beta on each side of the boundary. We set $B_{01} \perp B_{02}$ in region A, $B_{01} \parallel B_{02}$ in regions B and C. We have investigated unbounded magnetospheric cases applicable to regions A, B, and C. We also examined cases of a bounded magnetosphere, for regions A and B, where the inner boundary is set at $d = 9R_E$ in region A, and at $d = 17R_E$ in region B. Note that the results of unbounded region B also apply to unbounded region C since the magnetic field and the background flow velocity configurations are the same for these two regions. All the physical values are calculated in the stationary frame of the plasmas on either side of the magnetopause. Since the background flow is set to zero in region 2, the stationary plasma frame is also the magnetospheric stationary frame such that $\omega_2' = \omega$.

Table 1. Magnetic Field Configurations for Regions A, B, and C[a]

Regions								
A			B			C		
θ_1	θ_2	d	θ_1	θ_2	d	θ_1	θ_2	d
0°	90°		0°	0°		0°	0°	
30°	60°		30°	30°		30°	30°	
45°	45°	9	45°	45°	17	45°	45°	∞
60°	30°		60°	60°		60°	60°	
90°	0°		90°	90°		90°	90°	

[a] θ_1 and θ_2 represent the direction of wave propagation with respect to the background magnetic fields in the magnetosheath and the magnetosphere, respectively, and d is the distance to the inner boundary, where appropriate.

3. Results

[16] In this section, KH surface modes excited by the shear flow TDs with five different wave propagation directions with respect to the background magnetic fields will be considered in regions A, B, and C of the magnetosphere. The magnetic field orientations are summarized in Table 1. All of the generated MHD modes have been investigated, and the KHI-related modes examined in the context of wave-wave interactions and their relation to the primary and secondary KHI and to negative energy waves. The MHD waves will be classified as slow and fast modes based on their phase velocity with respect to the Alfvén speed using phase velocity diagrams, i.e., Friedrichs diagrams, and the effect of the background flow on the phase velocity in the magnetosheath will be displayed through these diagrams as well. Significantly, the importance of the primary and secondary KHI waves under different conditions along the magnetopause in regions A, B, and C, will be summarized and compared to previous satellite observations.

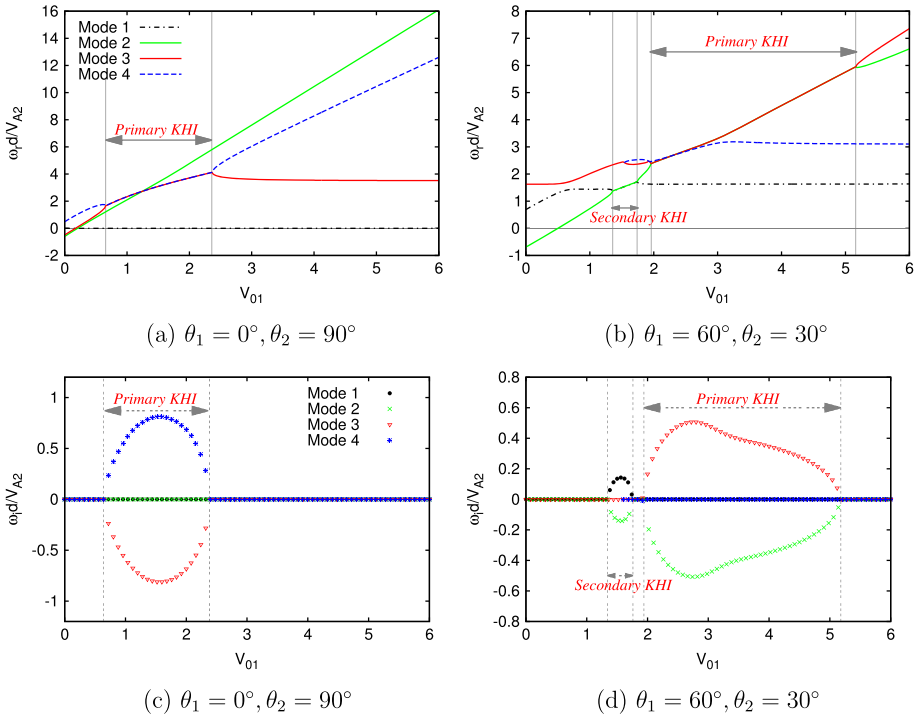

(a) $\theta_1 = 0°, \theta_2 = 90°$ (b) $\theta_1 = 60°, \theta_2 = 30°$

(c) $\theta_1 = 0°, \theta_2 = 90°$ (d) $\theta_1 = 60°, \theta_2 = 30°$

Figure 3. (a and b) Real frequencies and (c and d) growth rates of two different configurations of region A for the case of unbounded magnetosphere. Modes are labeled 1–4 for clarity. For each configuration, where different modes have equal real frequencies and are in complex conjugate pairs, this implies the presence of linear wave-wave interactions and the possibility of instability. Positions of KHI onsets and upper cut-off velocities are marked with vertical lines and primary and secondary KHI intervals are labeled.

3.1. Growth Rates and Frequencies

[17] For the case of an unbounded shear flow interface, the KHI can be understood through the linear mode interactions that can occur when the waves have equal frequencies and wave numbers, i.e., when they have equal phase velocities [e.g., *Swanson*, 1989; *Shiryeava*, 2001]. Across our warm plasma interface, four physically distinct modes (numbered from 1–4 for clarity) associated with the KHI are obtained with the set of the parameters listed in Table 1. The real frequencies and growth rates corresponding to $\theta_1 = 0°, \theta_2 = 90°$ (Figures 3a and 3c) and $\theta_1 = 60°, \theta_2 = 30°$ (Figures 3b and 3d) for an unbounded magnetosphere are shown in Figure 3 as examples illustrating the characteristics and physical aspects of the interacting MHD modes. This is equivalent to an unbounded case of region A. Here θ_1 and θ_2 are the angles of propagation with respect to the background magnetic field in regions 1 and 2, respectively. In Figure 3 the real frequencies (top row) are shown with solid lines and the growth rates (bottom row) are shown with symbols; the growth rate of a specific mode is shown with the same color as its real frequency. Since magnetic tension was present for all the cases presented in Figure 3, a lower cut-off velocity, that is a background flow velocity value above which KHI onset occurs, always existed. The primary and the secondary KHI intervals are marked with vertical lines and corresponding labels. For this unbounded case, mode interaction regions are observable when two modes have equal real frequencies, ω_r, and growth rates, ω_i, in complex conjugate pairs. For each unbounded configuration, KH instability occurs when two linear wave modes can be considered to interact; in Figure 3a modes 3 and 4 are interacting, while in Figure 3b, modes 3 and 2 are interacting throughout the primary KHI interval. It is also seen in Figures 3c and 3d that these interacting modes have complex frequencies in complex conjugate pairs as expected.

[18] The secondary KHI does not exist in Figure 3 for $\theta_1 = 0°, \theta_2 = 90°$, but is present for the configuration of $\theta_1 = 60°, \theta_2 = 30°$ in the interval of instability with lower V_{01}. Figure 3b shows that the secondary KH instability occurs when modes 1 and 2 are interacting, again in complex conjugate pairs. The phase velocity of these wave modes are also calculated and found to be equal to each other, as expected, throughout intervals of the primary and secondary KHI. In this unbounded case, there is an upper cut-off speed for both the primary and secondary KHI. The real frequencies and growth rates of the surface wave modes obtained for the unbounded ($d \to \infty$) cases of the nightside and the magnetotail configurations in regions B and C display similar characteristics to those in Figure 3.

[19] When an inner boundary is included, however, the KH unstable modes no longer occur in complex conjugate pairs and can have different frequencies. Therefore, the concept of linear wave-wave interactions are not valid in the case of a bounded magnetosphere. This fact is illustrated in Figures 4a and 4c for a bounded dayside magnetosphere for $\theta_1 = 90°, \theta_2 = 0°$ (region A) and in Figures 4b and 4d for a bounded nightside magnetosphere for $\theta_1 = \theta_2 = 60°$ (region B). It is seen in Figures 4c and 4d that the KHI still exists in

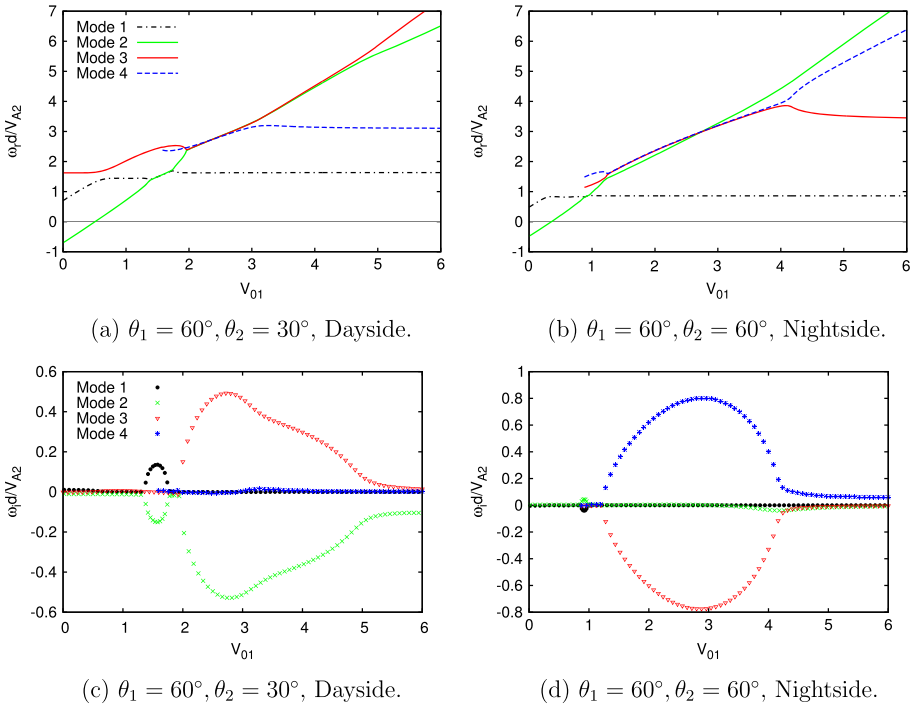

(a) $\theta_1 = 60°, \theta_2 = 30°$, Dayside. (b) $\theta_1 = 60°, \theta_2 = 60°$, Nightside.

(c) $\theta_1 = 60°, \theta_2 = 30°$, Dayside. (d) $\theta_1 = 60°, \theta_2 = 60°$, Nightside.

Figure 4. Growth rates and real frequencies for a bounded magnetosphere. (a and c) Results for bounded dayside flanks, region A. (b and d) Results for bounded nightside flanks, region B. It is clearly seen that the unstable modes are no longer characterized by complex conjugate pairs, and the real frequencies of the stable and unstable branches are not exactly equal.

the bounded case, but with the exclusion of an upper cut-off velocity, i.e, once a mode becomes unstable it remains unstable even though the growth rate decreases as the background flow speed increases. Physically, this can be understood to arise from the fact that waves can now be reflected from the bounded magnetosphere and influence the instability conditions at the shear flow magnetopause boundary. As in the semi-infinite magnetosphere case, stable nongrowing waves are present before the onset of the primary and secondary KHI. Such stable MHD surface wave modes could potentially still be excited on the magnetopause by processes such as solar wind dynamic pressure perturbations at flow speeds below the onset of the KHI. Figure 4c displays the additional feature that for the configuration $\theta_1 = 60°, \theta_2 = 30°$, the magnetic tension is not strong enough to quench the KHI so that mode 1 has a small growth rate even for very small flow speed. For the bounded case, it seems likely that the effects of magnetospherically reflected waves can cause the waves to become KH unstable even at very low background flow speeds.

[20] In the semi-infinite magnetosphere case, complex conjugate pair wave-wave interactions is possible throughout the primary and the secondary KHI intervals, and for flow speeds above the unstable region, all the modes have different frequencies and are purely propagating with zero growth rates (see Figure 3 as an example). For the bounded magnetosphere, however, the wave modes are not in complex conjugate pairs anymore and do not have equal real frequencies, implying that the two mode complex conjugate wave-wave interaction does not hold anymore, and thus, the upper cut-off speed does not exist (see Figure 4 as examples from our results). We suggest that the absence of complex conjugate pairs and thus symmetric wave-wave interactions, are the reason for the removal of the upper cut-off speed in the bounded magnetosphere case. The fact that the KHI occurs in the bounded magnetosphere case, although there are no symmetric wave-wave interactions, also indicates that the onset of the KHI is not related to the two wave interactions in contrast to what has been previously suggested [*Taroyan and Erdélyi*, 2003a, 2003b, 2002; *Mills et al.*, 1999; *Cairns*, 1979].

[21] All of the other configurations in Table 1 demonstrate a similar distinction between the unbounded magnetosphere and bounded magnetosphere.

3.2. Doppler Shifted Frequencies: Are KHI Relevant Waves Negative Energy Waves?

[22] Negative energy waves or over-reflected waves have been suggested to have negative Doppler-shifted frequencies [e.g., *Mann et al.*, 1999; *McKenzie*, 1970]. Our results show that the Doppler-shifted frequencies of unstable wave modes have negative values after the onset of the primary and secondary KHI, implying that they are negative energy waves. This result agrees with the previous results by *Pu and Kivelson* [1983a] and *Mann et al.* [1999] that the KHI waves always have negative energy. This fact is displayed in Figure 5a for an unbounded magnetosphere with magnetic field configuration $\theta_1 = 60$, $\theta_2 = 30°$, and in Figure 5b for a bounded magnetosphere with magnetic field configuration $\theta_1 = \theta_2 = 30°$, representative of regions A and B, respectively. In Figure 5, normalized doppler shifted frequencies are shown such that, $\omega_{\text{doppler}} = \omega_r d/V_{A2} - \mathbf{V_{01}}.\mathbf{k_t} d$. In the unbounded case, for flow speed above the upper cut-off speed, previously KH unstable modes still have a negative

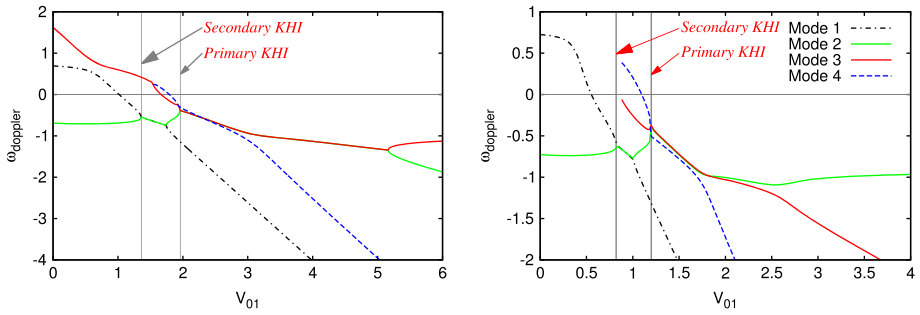

(a) $\theta_1 = 60°, \theta_2 = 30°$, Day-side. (b) $\theta_1 = 30°, \theta_2 = 30°$, Night-side

Figure 5. Normalized doppler shifted frequencies, $\omega_{\text{doppler}} = \omega_r d/V_{A2} - \mathbf{V_{01}}.\mathbf{k_t} d$ (a) for region A for an unbounded magnetosphere with $\theta_1 = 60°$, $\theta_2 = 30°$ and (b) for region B for a bounded magnetosphere with $\theta_1 = 30°$ and $\theta_2 = 30°$. All the modes have negative Doppler shifted frequencies after the onsets of the primary and secondary KHI. Vertical lines mark the flow speed for the onset of the primary and secondary KHI.

Doppler shifted frequency (see Figure 5a). Therefore, a negative Doppler shifted frequency (and negative energy waves) is a necessary, but not sufficient, condition for the KHI to be unstable. However, extraction of energy from the background flow by the waves remains responsible for the onset of the KHI.

[23] *Walker* [2000] offers an attractive alternative approach, where energy exchange between the waves and the background flow is considered instead of emphasizing the negative energy of the waves. In *Walker* [2000], the energy extraction is also shown to be possible through the work done on the wave by the background flow, which can be explained and is dependent on the Reynolds and Maxwell stresses on the boundary. Following *Walker* [2000]'s idea, we believe that the K-H unstable waves also extract energy from the background flow through the work done by the Maxwell and Reynolds stresses. In order to fully explain the relationship between the KHI, negative energy waves and work done by the stresses at the boundary, further work is needed using the approach suggested by *Walker* [2000] and this is left as a future work.

3.3. Characteristics of KH Unstable MHD Modes: Dependence on the Angle of Propagation

3.3.1. Phase Velocity Diagrams

[24] In this section, the angles of propagation, θ_1 and θ_2, in the two media are varied from 0 to 2π while the magnetic field and flow velocity orientations are maintained constant. This allows the classification of the wave modes as fast and slow by comparing their phase velocities with the Alfvén speed using phase velocity diagrams. The total phase velocity of the modes are plotted in a polar coordinate system with their magnitude along **k** with respect to the background field direction (i.e., in the form of Friedrichs diagrams). For each different value of propagation angle, the total phase velocity is calculated using the solution for the frequencies and wave numbers from the dispersion relation, with the equation

$$\mathbf{U_p} = \frac{\omega_r}{(k_t^2 + k_x^2)}\mathbf{k}. \tag{8}$$

[25] Normalized phase velocity, $V_p = U_p/V_{A2}$, diagrams of KHI relevant MHD modes for the dayside magnetosheath and magnetosphere, region A, are shown in Figure 6 at flow velocity value $V_{01} = 2.3$. The phase speeds for decoupled Alfvén modes propagating at the Alfvén speed in each media are shown in each diagram both for comparison and for classifying modes as slow or fast. These Friedrichs diagrams aid with understanding the behavior of the MHD modes in the magnetosheath and magnetosphere, which are coupled across the magnetopause under the influence of background plasma flow. Figures 6a show that in the magnetosheath, the phase velocity of the modes is distorted due to the effects of the background flow and coupling to the modes in the magnetosphere.

[26] Figure 6b displays that in the magnetosphere, only mode 1 is a slow mode for all propagation angles and all the other modes have fast mode characteristics. Interestingly, for the same flow speed Figure 6b also shows that mode 2 and 4 become slow modes at values of $\theta_2 \lesssim 30°$. The intervals of the primary KHI are highlighted with grey colors and those of the secondary KHI are highlighted with yellow colors. The primary KHI which holds for the propagation angles $\theta_2 \simeq 26° - 90°$ for the first quadrant of Figure 6b; the other three quadrants are symmetric with respect to the first quadrant. Throughout this interval, mode 3 is the unstable mode at $\theta_2 \simeq 26° - 32°$ and is interacting with mode 2, and mode 4 is unstable at $\theta_2 \simeq 33° - 90°$ and is interacting with mode 3. The secondary KHI holds for propagation angles $\theta_2 \simeq 19° - 24°$, where mode 1 is unstable and is interacting with mode 2. Remembering the result found in section 3.1 that in an infinite unbounded medium, the wave-wave interaction is related to both primary and secondary KHI, Figure 6b shows that in region A of a semi-infinite dayside magnetosphere, the primary KHI is related to a fast-fast mode interaction and the secondary KHI is related to a slow-slow mode interaction in the magnetosphere. Of course the mode interaction (overlap) is seen in both the magnetosphere and magnetosheath on either side of the shear flow boundary.

[27] Interestingly, of course, the modes can have different fast or slow characteristics on either side of the magnetopause. For example the secondary KHI wave seen in Figures 6a and 6b (at low θ_2) is a slow mode in the magnetosphere, but a fast in the magnetosheath. For the primary KHI it is a fast mode in both magnetosphere and magnetosheath.

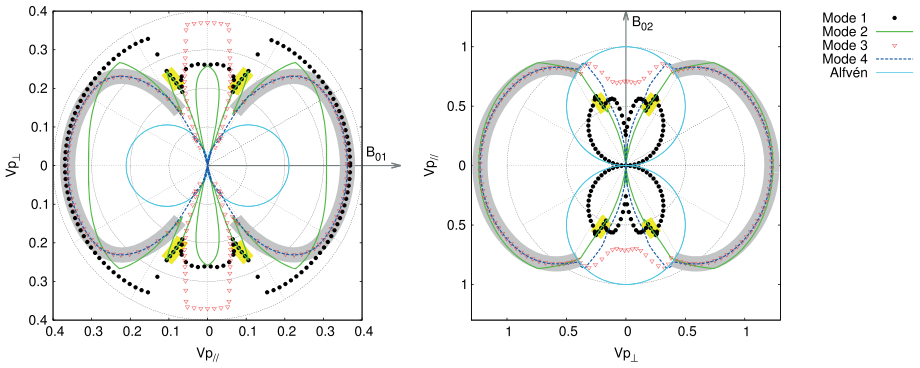

(a) $V_{01} = 2.3$, Magnetosheath modes (b) $V_{01} = 2.3$, Magnetosphere modes

Figure 6. Friedrichs phase speed (normalized by V_{A2}) diagrams at flow velocity value 2.3 for dayside unbounded region A, (a) in the magnetosheath, and (b) in the magnetosphere. Wave mode 3 is a fast mode in the magnetosphere at angles of propagation $\theta_2 \simeq 30° - 90°$, and its phase velocity is smaller than the Alfvén wave at angles $\theta_2 \simeq 0° - 30°$. Modes 2 and 4 are fast for $\theta_2 \gtrsim 30°$ and slow for $\theta_2 \lesssim 30°$ angle of propagation. In the magnetosheath, all the modes are fast modes at all values of θ_1. Yellow shaded areas mark the secondary KHI zones and grey shaded areas mark the primary KHI zones.

[28] The results for the bounded dayside magnetosphere are morphologically similar to the unbounded cases shown in Figure 6, despite the fact that perfect wave-wave interactions do not occur in the bounded case. To illustrate this point, phase velocity diagrams for unbounded and bounded dayside magnetosphere flanks, with other parameters from region A, are shown in Figures 7a and 7b, respectively, for $V_{01} = 1.6$. The primary and secondary KHI zones are again marked with grey and yellow highlights. In Figure 7a (the unbounded case), mode 4 is unstable to the primary KHI for $\theta_2 \simeq 32° - 90°$ and it has a phase velocity equal to that of mode 3 throughout this interval. Whereas, in Figure 7b, these two modes propagate at different phase velocities although mode 4 is still unstable to the primary KHI at about the same range of angles as in Figure 7a. Similarly, mode 1 is unstable to the secondary KHI for $\theta_2 \simeq 26° - 32°$ in both unbounded and bounded magnetosphere cases and it has equal phase velocity to that of mode 2 only in the unbounded case. Despite the fact that symmetric complex conjugate wave-wave interactions do not occur in the bounded case, there remains regions of primary and secondary KHI. Therefore, in the bounded magnetosphere, the upper cut-off velocity is removed and boundary is never again perfectly stabilized with increasing flow speed once it becomes unstable.

[29] Example Friedrichs diagrams of MHD modes for the unbounded magnetotail, region C, are shown in Figure 8 for the magnetosheath and the magnetosphere at magnetosheath flow velocity values $V_{01} = 1$ and 2.3. A new result shown in Figure 8 is that none of the modes propagate perpendicular to the background magnetic fields, and hence, also perpendicular to the magnetopause boundary. Hence, the MHD waves in the magnetotail cannot have **k** exactly perpendic-

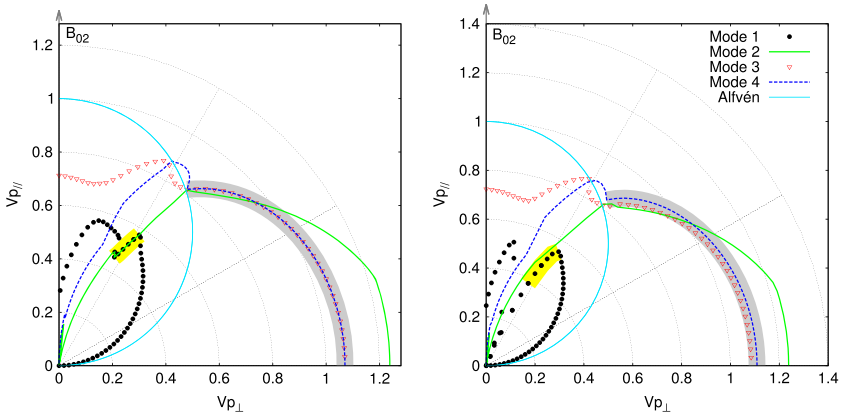

(a) Unbounded (b) Bounded

Figure 7. Friedrichs (normalized) phase speed diagrams at flow velocity value $V_{01} = 1.6$, on the magnetosphere side of region A, (a) semi-infinite and (b) bounded magnetosphere respectively, displaying the presence/absence of linear wave-wave mode interaction in each case.Throughout the primary and secondary KHI intervals, grey and yellow shaded areas, modes 3 and 4 and modes 1 and 2 have exactly equal phase velocity for a semi-infinite magnetosphere while they are propagating at different phase velocities for a bounded magnetosphere.

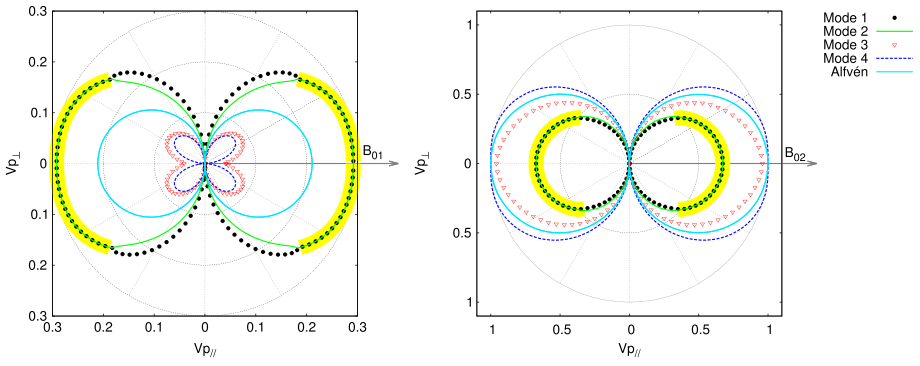

(a) $V_{01} = 1$, Magnetosheath modes (b) $V_{01} = 1$, Magnetosphere modes

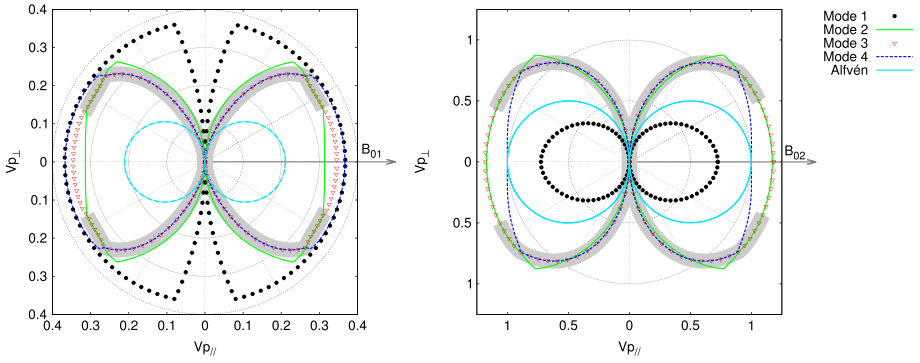

(c) $V_{01} = 2.3$, Magnetosheath modes (d) $V_{01} = 2.3$, Magnetosphere modes

Figure 8. Normalized phase velocity diagrams at two different flow velocity values for region C, for (a and c) the magnetosheath, and (b and d) the magnetosphere. Only secondary KHI is obtained in Figures 8a and 8b, yellow shaded areas, and only primary KHI is obtained in Figures 8c and 8d, grey shaded areas. Characteristics of the wave propagation are significantly different than that in region A; specifically, perpendicular propagation of the modes does not occur on either side of the magnetopause, which introduces a new type of modes labeled intermediate-fast modes in this paper (see text for details).

ular to $\mathbf{B}_{01,02}$, such that they must propagate either sunward or antisunward with a component of phase speed parallel or antiparallel to $\mathbf{B}_{01,02}$. These type of surface modes have been obtained in the past when a background plasma flow is present [e.g., *Tajiri*, 1967; *Kato et al.*, 1966, *Namikawa and Hamabata*, 1981]. These wave modes are considered to be a type of mixed fast-slow modes which we call intermediate-fast modes following the terminology of *Namikawa and Hamabata* [1981]. Intermediate-fast modes are defined in this paper as the modes that have phase velocity values in the expected range of fast mode waves but do not propagate exactly perpendicular to the background magnetic field.

[30] Figures 8a and 8c show that, on the magnetosheath side, modes 3 and 4 convert to intermediate-fast from slow modes as flow velocity increases, while mode 1 and 2 stay as intermediate-fast. On the magnetosphere side, modes 2 and 3 are generated as slow modes and converted to intermediate-fast modes as the flow velocity increases, while mode 1 is generated and remains as a slow mode in Figures 8b and 8d. Mode 4 is also a slow mode for flow velocity values $V_{01} < 1$ and converts to intermediate-fast at larger flow speeds. Mode interaction zones match with the intervals of the primary and secondary KHI, grey and yellow shaded areas, and are similar to those shown for the dayside magnetosphere flanks, region A, in Figure 6. Figure 8b shows that in the magnetosphere, at flow velocity $V_{01} = 1$, both modes 1 and 2 are slow modes and are interacting with each other during the secondary KHI interval. Again these same modes show a fast-fast interaction on the magnetosheath side.

[31] Friedrichs diagrams of the MHD modes obtained on the bounded nightside magnetosphere flanks, region B, show similar characteristics to those in region C in the magnetotail. However, due to the presence of the inner boundary for bounded region B, perfect linear two wave-wave interactions are not obtained in regions of instability due to the impact of reflected modes and their interaction at the shear flow boundary. Figure 9 shows the Friedrichs diagrams for wave modes in the magnetosheath, for regions C and B, to enable a comparison of wave-wave interaction in the unbounded and bounded magnetotail similar to that shown for region A in Figure 7. In Figure 9, only secondary KHI holds and intervals are highlighted with yellow colors as well. In Figure 9a, mode 1 is unstable for the propagation angles of $\simeq$ 0° – 80° and is interacting with mode 2 throughout this interval, i.e, has equal phase velocity. While in Figure 9b, although mode 2 is unstable for the propagation angles $\simeq$ 0°–88°, it does not show linear wave-wave interactions with mode 1 or with any other existing modes. Figures 9c and 9d also show similar characteristics for the case where the background flow value $V_{01} = 1$, where mode 1 is unstable for $\theta_1 = 0° - 42°$ in Figure 9c, and mode 2 is unstable for $\theta_1 = 0° - 45°$ in Figure 9d. Again there are no wave-wave interactions in the bounded case

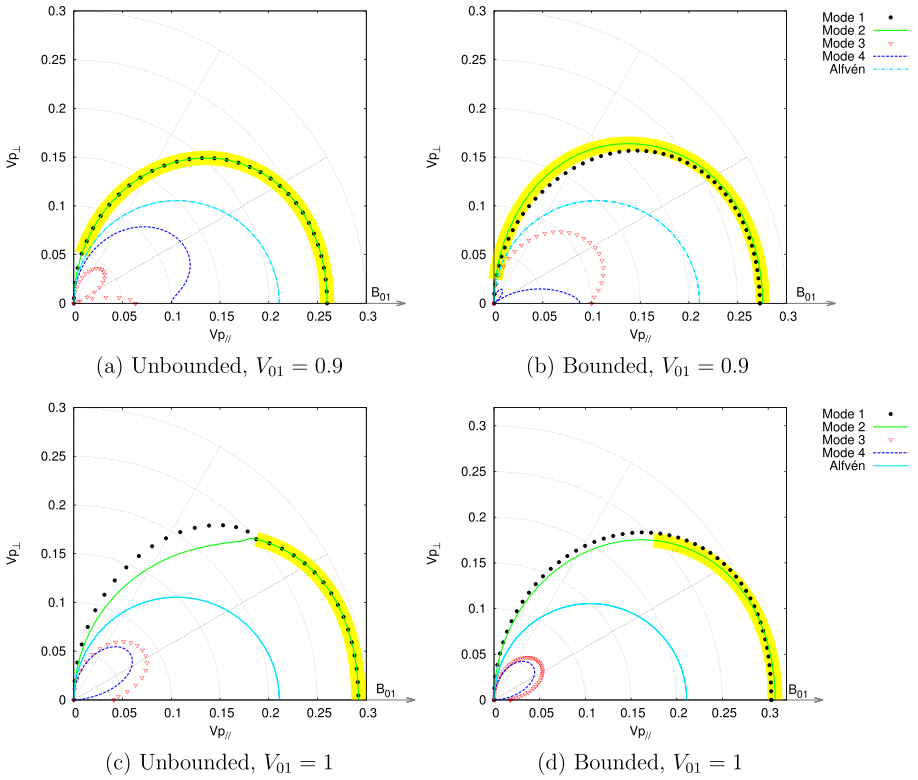

(a) Unbounded, $V_{01} = 0.9$ (b) Bounded, $V_{01} = 0.9$

(c) Unbounded, $V_{01} = 1$ (d) Bounded, $V_{01} = 1$

Figure 9. Friedrichs (normalized) phase speed diagrams in the magnetosheath at two background flow values: (a and b) $V_{01} = 0.9$, and (c and d) $V_{01} = 1$. (left) Region C (unbounded) and (right) region B (bounded). Secondary KHI regions, which is the only present instability at these flow speeds, are highlighted with yellow colors. The presence/absence of the linear wave-wave interactions in the semi-infinite/bounded case representing region C/B are clearly seen (see text for details).

of Figure 9d, while modes 1 and 2 are linearly interacting through complex conjugate pairs throughout the secondary KHI zone in Figure 9c. Note that while modes 1 and 2 are intermediate fast waves at these flow velocity values on the magnetosheath, they are slow waves on the magnetosphere side at the background flow speeds shown in Figure 9 (see Figure 8b for $V_{01} = 1$ as an example). Figure 9a also shows that the phase speed of mode 3 diminishes at $\theta_1 \simeq 30°$, on the magnetosheath side, where the phase velocity is either zero or purely imaginary, and the wave propagation direction changes from upstream to downstream.

3.3.2. Growth Rate Dependence on the Angle of Propagation

[32] A polar plot of the growth rates of the unstable modes with respect to the propagation angle is shown in Figure 10 for the semi-infinite magnetosphere case with B_{01} perpendicular to B_{02} as in region A with $V_{01} = 2.3$. At this value of the background flow, both the primary and the secondary KHI are possible at different values of the angle of propagation. Figure 10 shows that at this value of the background flow velocity, the primary KHI is generated by mode 3 for $\theta_2 \simeq 26° - 32°$ and by mode 4 for $\theta_2 \simeq 33° - 90°$ in the first quadrant. The secondary KHI is generated purely by mode 1 at $\theta_2 \simeq 19° - 23°$. It is also visible on Figure 10 that the growth rates of the primary KHI peak around $\theta_2 = 45°$, and that of the secondary KHI peak at $\theta_2 = 22°$, where θ_2 is the angle of propagation with respect to the magnetic field in the magnetosphere, B_{02}. Exactly the opposite holds for propagation angles (θ_1) with respect to the magnetic field in the magnetosheath, B_{01}. The bounded magnetosphere case for region A (not shown) displayed very similar characteristics as the unbounded magnetosphere case presented in Figure 10.

[33] For regions B and C, there is not a single flow velocity at which both the primary and secondary KHI are obtained simultaneously. Therefore, the primary KHI growth rate is calculated at the background flow velocity value $V_{01} = 2.3$, and the secondary KHI growth rates are calculated at $V_{01} = 1$. Both are plotted for clarity in Figure 11 for region C. The primary KHI growth rates are caused partially by mode 3 and partially by mode 4 similar to Figure 10; mode 3 is unstable at $\theta_1 = \theta_2 \simeq 23° - 40°$ and mode 4 is unstable at $\theta_1 = \theta_2 \simeq 40° - 90°$. Figure 11 shows that the primary KHI growth rates peak at $\theta_1 = \theta_2 \simeq 56°$, and secondary KHI growth rates peak at $\theta_1 = \theta_2 \simeq 0°$. There is no unstable mode at $\theta_1 = \theta_2 = 90°$ which is expected since there is no propagating mode at this direction for region C. The growth rate characteristics for region B (not shown) displayed similar characteristics to those for region C shown in Figure 11.

3.4. Energy Propagation Into the Magnetosphere With the Primary and Secondary KHI Waves

[34] The direction of energy propagation resulting from KH unstable modes can be understood using polar group

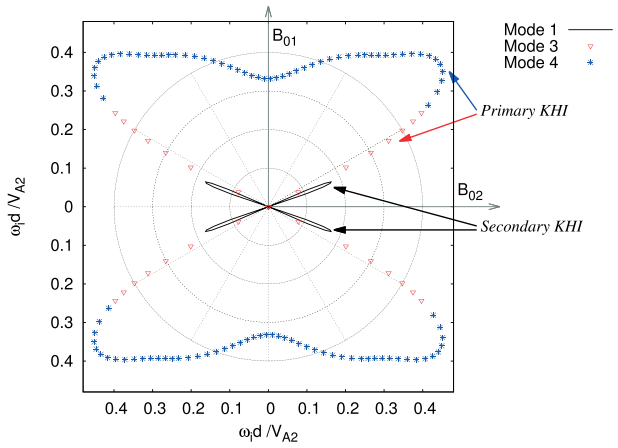

Figure 10. Growth rate dependence on the angle of propagation for $V_{01} = 2.3$, in region A for a semi-infinite magnetosphere. Primary and secondary KHI regions are labeled and the background magnetic field orientations in the magnetosheath and magnetosphere are shown with arrows. At this flow velocity, the primary KH instability is caused by modes 3 and 4, shown with red triangles and blue points, at different propagation angles. Secondary KHI is caused by mode 1 and is shown with black lines. Primary instability growth rate peaks at orientation angles $\simeq 45°$, and secondary growth rate peaks at $\simeq 22°$, with respect to B_{02} on the magnetosphere side, while exactly the opposite holds with respect to the B_{01} on the magnetosheath side. Primary KHI is possible at a wide range of angles $\simeq 30° - 90°$, while secondary KHI only occurs at $\simeq 19° - 23°$.

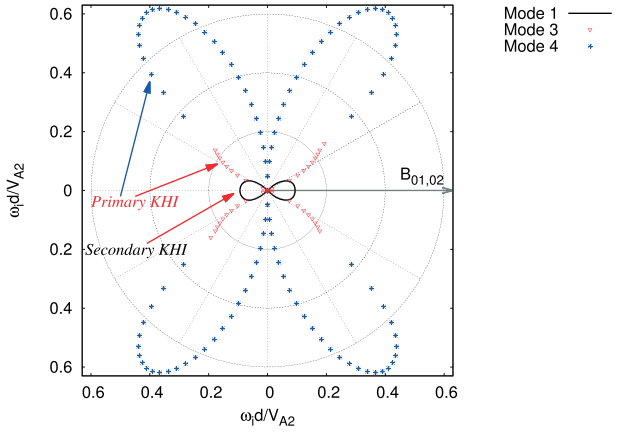

Figure 11. Growth rate dependence on the angle of propagation in the magnetotail, region C, for the primary and secondary KHI. The results for the primary KHI were obtained at flow velocity value $V_{01} = 2.3$, and for the secondary KHI were obtained with $V_{01} = 1$. The growth rate of the secondary KHI peaks about 0°, and the growth rate of the primary KHI peaks at about 56°, with respect to the direction of the background magnetic fields, B_{01} and B_{02}. Growth rates are zero at 90° propagation angle for both the primary and the secondary KHI.

velocity Friedrichs diagrams. Group velocities are calculated using the following equation:

$$U_{gr} = \frac{d\omega}{dk},$$

and normalized group velocities are plotted, which is $V_{gr} = U_{gr}/V_{A2}$. These are shown in Figure 12 for region A for a semi-infinite magnetosphere with the same value of background flow speed from Figure 6. Since our primary interest is investigating energy propagation into the magnetosphere from the magnetosheath, the group velocities are calculated only for the magnetosphere. In Figure 12, the primary KH unstable mode consists partially of mode 3 and partially of mode 4, depending on the angle of **k**, while the secondary KH unstable mode is mode 1(see Figure 6 and the text related to it for details). Normalized group velocity diagrams of primary KHI modes in Figures 12 shows that modes 3 and 4 are able to propagate energy perpendicular to the background magnetic field in region A. However, these modes have zero group velocity at a small range of angles $\theta_2 \simeq 0°$, and thus cannot propagate energy along this direction. The secondary KHI is only obtained in Figure 12 for θ_2 between $19° - 23°$ and is caused by mode 1. The Figure 12 hence shows that secondary KH modes can propagate energy into the magnetosphere only at a very narrow range of angles of propagation.

[35] In regions B and C, although the phase velocity diagrams have shown that the primary and the secondary KHI waves are not able to propagate purely perpendicular to the background magnetic field and the phase velocity values become comparably small as the propagation angles approach to 90°, the group velocity diagrams do not show the same characteristics due to the behavior of the intermediate-fast modes, in this case and discussed earlier. Figure 13 shows an example of this for region C. In Figure 13a, the secondary KH unstable mode is mode 1 and the primary KHI is not obtained for this background flow at all. Figure 13a shows that for $V_{01} = 1$, mode 1 has a group velocity comparable to its phase velocity across a wide-range of angles of propagation, and can propagate energy in these directions. The primary KHI is obtained once the

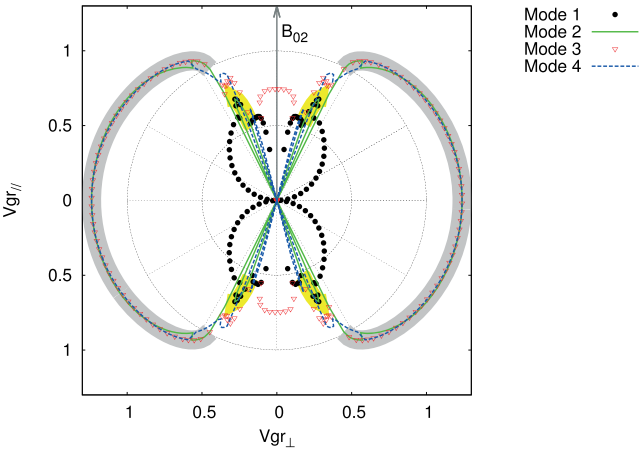

Figure 12. Group velocity (normalized by V_{A2}) diagrams at flow velocity value $V_{01} = 2.3$ in region A for a semi-infinite magnetosphere. The yellow and grey shaded areas mark the secondary and primary KHI intervals, the same as in the corresponding phase velocity diagrams shown on Figure 6.

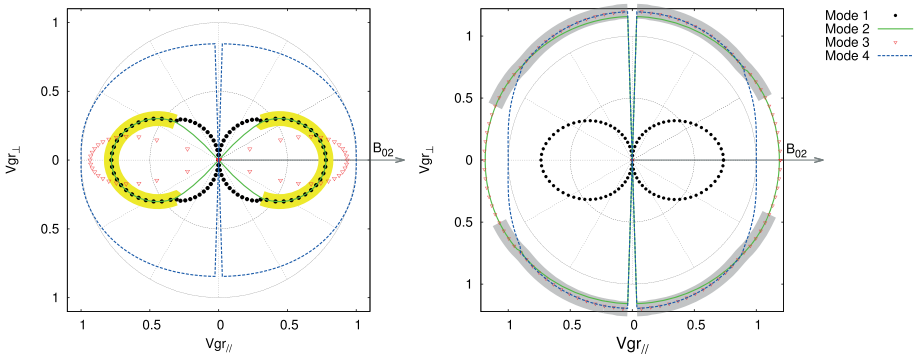

(a) $V_{01} = 1$ (b) $V_{01} = 2.3$

Figure 13. Normalized group velocity diagrams for (a) $V_{01} = 1.0$, and (b) $V_{01} = 2.3$ in region C for a semi-infinite magnetosphere. The same as in the corresponding phase velocity diagrams (see Figure 8), the primary and secondary KHI intervals are marked with grey and yellow colors, respectively.

flow speed is fast enough and at $V_{01} = 2.3$ it is seen to be caused partially by mode 3 and partially by mode 4 as shown in Figure 13b (see also section 3.3.1, Figure 8, and the text related to it). The group velocities of modes 3 and 4 have high values at all angles of propagation except for a very narrow range of angles close to 90°, which shows that the energy transport is very efficient by these modes at these highly oblique angles despite the small values of phase speed. Exactly at $\theta_2 = 90°$, where intermediate-fast modes have zero phase speed, the group speed is undefined.

[36] We have also investigated the normal and the parallel phase velocities of the modes in order to investigate the energy transport by the primary and secondary KHI modes as flow velocity increases. All of the modes have zero normal components of phase speeds at low shear flow velocity where neither secondary nor primary KHI lower cut-off velocities have been reached. The modes start to pick up finite perpendicular phase speeds at the onsets of the primary and secondary KHI. This fact is displayed in Figure 14a for $\theta_1 = 30°, \theta_2 = 60°$ representing region A, and Figure 14b for $\theta_1 = 30°, \theta_2 = 30°$, representing region C, for a semi-infinite magnetosphere. The primary KH instability is caused by mode 4 in Figure 14a, and by mode 3 in Figure 14b. Both of these modes have zero normal phase speeds before, and they pickup large normal speeds after the onset of the KHI. After the upper cut-off velocity is reached, the normal phase velocity of mode 4 decreases to a constant value while that of mode 3 continues to increase. This result suggests that propagation and energy transport away from the magnetopause may be efficient due to the waves excited by the primary KHI.

[37] The secondary KHI is caused by mode 1 in Figures 14a and 14b and it also picks up a finite normal phase speed after the KHI onset, however, it is significantly smaller than the normal speed of the primary KHI waves. After the upper cut-off velocity is reached, the normal phase speed of the secondary KHI mode decreases to zero, suggesting that energy transport due to the secondary KHI is mainly possible only during the narrow KHI unstable interval. Nevertheless, since under certain slow values of the background magnetosheath flow, the secondary KHI may be the only active instability, it could be the only means of extracting energy from the flow, and thus, it could still be dynamically important. With the difference between the perpendicular phase speeds, it is possible that such characteristics may provide a diagnostic mechanism for distinguishing between the primary and secondary KHI waves. The wave propagation characteristics of the primary and the secondary KHI

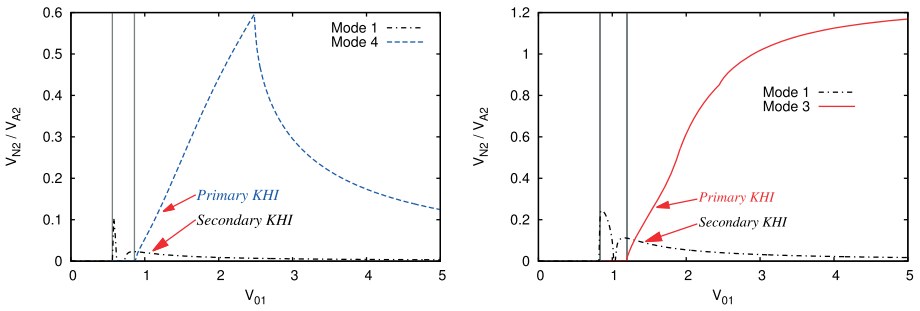

(a) Region A (b) Region C

Figure 14. Normal phase velocities of the primary and secondary K-H unstable modes for semi-infinite magnetosphere with magnetic fields orientations (a) $\theta_1 = 30°, \theta_2 = 60°$, corresponding to region A, and (b) $\theta_1 = 30°, \theta_2 = 30°$, corresponding to region C. Onsets of the primary and the secondary KHI are marked with vertical lines. Primary KHI is caused by mode 4 in Figure 14a and mode 3 in Figure 14b, and the secondary KHI is caused by mode 1 in both Figures 14a and 14b.

Table 2. In Situ Satellite Observations of KH Surface Waves[a]

Paper	Region	U_{01}(km/s)	V_{A2}(km/s)	V_p (km/s)	V_p/V_{A2}	U_{01}/V_{A2}
[*Agapitov et al.*, 2009]	A	290 – 310	264	190 – 240	0.7 – 0.9	1.1 – 1.2
[*Hasegawa et al.*, 2006]	A	250	500	150	0.3	0.5
[*Gnavi et al.*, 2009]	B	300	308	200	0.7	1
[*Owen et al.*, 2004]	B	100 – 200	163	65	0.4	0.6 – 1.2
[*Chen and Kivelson*, 1993]	B	200	327	106	0.3	0.6
[*Hwang et al.*, 2011]	C	538	436	322 – 400	0.7 – 0.9	1.2
[*Nakai and Ueno*, 2011]	C	330	308	50 – 250	0.1 – 0.8	1.07
[*Gnavi et al.*, 2009]	C	300	436	200	0.5	0.7
[*Foullon et al.*, 2008]	C	200	165	36 – 95	0.3 – 0.6	1.2
[*Hasegawa et al.*, 2006]	C	300	155	200	1.3	1.9
[*Fairfield et al.*, 2000]	C	338	209	230 – 250	1.1 – 1.2	1.6
[*Kivelson and Chen*, 1995]	C	560	655	320	0.4	0.9

[a] U_{01} is the background flow velocity in the magnetosheath, and $V_{01} = U_{01}/V_{A2}$ is the normalized value of U_{01} with respect to the background Alfvén speed in the magnetosphere. V_p is the phase velocity of the KHI waves, which are either directly given in the inspected papers or calculated using the given wavelengths and frequencies. Each published observation from the literature is also identified with one of regions, A, B, and C.

wave on the magnetopause are examined in detail in the following section.

3.5. Comparison to Observations

[38] In this section we compare our results to KHI observations from the literature. Specifically, we inspected various papers where KHI waves are observed in situ at the magnetopause and identified them with the three regions of the magnetosphere we have considered throughout this study, namely regions A, B, and C in Figure 1. The observed phase velocities of the waves and the Alfvén speed in the magnetosphere are calculated in km/s using the observed values reported in the papers. Background flow velocities at which the KHI waves are observed, and the phase velocities of these waves are normalized using the observed Alfvén speed in the magnetosphere in the same way as in this paper. The observational KHI papers examined and the values deduced from these observations are summarized in Table 2.

[39] Normalized phase velocity values from our results varied between $\simeq$ 0.3 – 1.2 in the magnetosheath, and $\simeq$ 0.5–1.3 in the magnetosphere, which are in general agreement with the observed phase velocity values of KHI waves summarized in Table 2. Combining the results of observations from Table 2 and global MHD simulation results from *Lavraud et al.* [2007] and *Lavraud and Borovsky* [2008], we can highlight a range of expected values of the normalized magnetosheath flow speed to generally vary between 0.5–1.3 in region A, 0.6–2.6 in region B, and 0.7–4 in region C. From our dispersion relation, which has a number of limitations including uniform plasma assumptions and an infinitely thin magnetopause, we can nonetheless identify that the intervals of the secondary KHI happens at normalized magnetosheath flow speed values of $\sim$ 0.7 – 1.8, and the intervals of the primary KHI happens at flow speed values of $\sim$ 0.8 – 4. This suggests that observed KHI waves in region A are mostly secondary KHI waves, and in regions B and C, they could be primary or secondary KHI waves. The peak values of the growth rates happen at background flow speeds $\sim$ 0.8 – 1.5 for the secondary KHI waves and at $\sim$ 1.5 – 2.9 for the primary KHI waves. These results suggest that if KH surface waves are seen on the near-Earth magnetopause, then the secondary KHI is a prime candidate, although secondary KHI is possible elsewhere too. Since the flow speed is usually smaller in region A, the primary KHI would be expected to be mainly observed in regions B and C. This could be the reason for relatively fewer observations of KHI waves in region A [*Hasegawa et al.*, 2006] than in regions B and C. Since the secondary KHI waves have relatively small growth rates and wave amplitudes in comparison to the primary KHI waves, they could also be detected less frequently. However, they can remain important since at low flow speeds, they are the only KH unstable waves and thus perhaps might be the only cause of energy transport via KHI in region A.

[40] Energy transport at the magnetopause might be mainly caused by the primary KHI in regions B and C since the magnetosheath flow may reach the lower cut-off for the primary KHI, and the peak values of the primary KH growth rates which are typically larger than those of the secondary KHI. Overall, this suggests that the energy transport due to the KHI are likely more efficient in regions B and C, since waves which grow to larger amplitudes can carry more energy into the magnetosphere. We have also compared the new result we found on the direction of KHI wave propagation in regions B and C; namely that propagation at angles exactly perpendicular to the background magnetic field, which in our case are exactly perpendicular to the magnetopause, is not possible. This agrees with observations of KHI wave propagation shown by *Foullon et al.* [2008], where the direction of observed KHI waves in region C varied between 50° – 86° either propagating sunward or antisunward (see Table 5 in their paper). We summarize in the form of a schematic, the general behavior of unstable primary and secondary KHI surface waves along the magnetopause in Figure 1.

4. Discussion and Conclusions

[41] In this paper, we have investigated the primary and secondary KHI surface wave phenomena in a warm homogeneous plasma in three regions of the magnetosphere, regions A, B, and C as shown in Figure 1. Our results show that the exclusion of the KH upper cut-off speed in a bounded magnetosphere is due to the interaction of magnetospherically reflected waves with the shear flow magnetopause boundary. In this case, unlike for an unbounded semi-infinite shear flow region, the unstable KH surface modes no longer occur in complex conjugate pairs. In the semi-infinite magnetosphere, wave-wave interactions

between the two complex conjugate pairs of modes, an exponentially growing and a decaying mode, are always allowed. These wave pairs have equal phase velocities and thus they can interact with each other throughout the KH unstable intervals. Since the linear and symmetric two wave mode interactions are not present in the bounded magnetosphere case due to the effects of the waves reflected from the inner boundary, the upper cut-off stabilization does not take place anymore.

[42] We identified the MHD surface waves as fast and slow waves by comparing their phase speed to the Alfvén speed through Friedrichs diagrams, i.e, phase velocity diagrams with respect to the direction of the background magnetic fields. On the dayside magnetosphere flanks, MHD waves are allowed to propagate in all directions. On the nightside magnetosphere flanks and in the magnetotail, waves cannot propagate exactly perpendicular to the magnetic field. They propagate in either sunward or antisunward directions and have the general characteristics of a fast mode but which cannot propagate exactly perpendicular to the background magnetic field and which we have described as intermediate-fast.

[43] The Doppler shifted frequencies of the primary and the secondary KH unstable surface waves are found to always have negative values. However, in contrast with [*Cairns*, 1979; *Mills et al.*, 1999; *Taroyan and Erdélyi*, 2002, 2003a, 2003b], our results indicated that linear interaction of a negative energy wave with a positive energy wave is not a necessary condition for the onset of the KHI. This is consistent with our suggestion that the onset of the KHI in the general case is not related to wave-wave interactions between complex conjugate pairs but to the extraction of energy by the wave from the background flow. This supports the suggestion by *Walker* [2000] that interestingly, the process of energy extraction from the shear flow is better described using the concept of work done by Maxwell and Reynolds stresses rather that in terms of negative energy waves. Further investigation of the relation between KH unstable MHD modes and energy exchange between the MHD wave modes and the background flow arising from work done by Maxwell and Reynolds stresses is left as a future work.

[44] The behavior of the primary and the secondary KHI unstable surface waves on the magnetopause is summarized in Figure 1. The phase velocity of the primary unstable KH waves have a large component perpendicular to the magnetopause once they become unstable. The group velocities show that energy propagation by unstable primary KHI wave modes is possible at all propagation angles, except for a very narrow range of the propagation angles close to 90° in regions B and C. Therefore, this wide range of the energy propagation angles shows that the energy propagation is likely to be more efficient when the primary KHI is active on the magnetopause. Regions B and C generally have background flow in the magnetosheath above the lower cut-off speed of the primary KHI, such that these regions are more liable to the primary KHI than region A. Energy transport into the magnetosphere from the magnetosheath are hence likely to be more efficient in regions B and C than in region A. The secondary unstable KH modes also have a finite but smaller perpendicular phase speed after the onset of the KHI. However, the value of this perpendicular component decreases with increasing flow speed above the peak value of the growth rate. Since the flow velocity in the magnetosheath in region A is mostly in the range of the lower cut-off velocity for the secondary KHI, the energy propagation via KHI in this region is mostly possible only with the secondary KHI waves. Comparison of our results to previously published in situ observations of the KHI surface waves also shows that the primary KHI is mostly possible on the nightside flanks and in the magnetotail, i.e, in regions B and C in Figure 1. In contrast, likely only the secondary KHI is possible in region A. Therefore, the energy transport into the magnetosphere from the magnetosheath is more efficient on the nightside flanks and in the magnetotail, in regions B and C, than in the nearer noon dayside flanks, in region A.

[45] Overall, the energy transport arising from the primary KH unstable surface wave is found to be more efficient than the secondary KHI, since the primary KHI waves have larger growth rates and larger phase speeds perpendicular to the magnetopause than the secondary KHI waves. On the magnetospheric side of the magnetopause, the primary KHI is caused by a fast wave and the secondary KHI is caused by a slow wave, which is consistent with our results showing that the secondary KH unstable surface wave generally propagates energy at a smaller range of propagation angles than the primary KHI surface wave.

[46] Future studies could examine the evolution of the KHI including the effects of a finite transition thickness layer at the magnetopause boundary, which would allow one to look at the waves at shorter wavelengths. This would help to develop a better understanding of the KHI phenomenon of magnetopause surface waves across a wider range of wavelengths. Allowing inhomogeneities in the magnetosphere would also provide better physical information on characteristics of the wave propagation into the magnetosphere, and an examination of the efficiency of the primary and secondary KHI in driving field line resonances in the magnetosphere. Finally, as discussed by *Mann et al.* [1999], the KHI may also be able to excite body (waveguide) modes in a bounded magnetosphere in addition to the surface waves examined here. The role of primary and secondary KHI in exciting KH unstable waveguide modes remains a subject for further study.

[47] **Acknowledgments.** I.R.M. and R.R. are supported by Discovery Grants from Canadian NSERC.

[48] Masaki Fujimoto thanks the reviewer for assistance in evaluating this paper.

References

Agapitov, O., et al. (2009), Surface waves and field line resonances: A THEMIS study, *J. Geophys. Res.*, *114*, A00C27, doi:10.1029/2008JA013553.

Allan, W., and A. N. Wright (1997), Large-m waves generated by small-m field line resonances via the nonlinear Kelvin-Helmholtz instability, *J. Geophys. Res.*, *102*(A9), 19,927–19,933.

Andries, J., and M. Goossens (2001), Kelvin-Helmholtz instabilities and resonant flow instabilities for a coronal plume model with plasma pressure, *Astron. Astrophys.*, *368*, 1083–1094.

Andries, J., W. J. Tirry, and M. Goossens (2000), Modified Kelvin-Helmholtz instabilities and resonant flow instabilities in a one-dimensional coronal plume model: Results for plasma $\beta = 0$, *Astrophys. J.*, *531*, 561–570.

Baumjohann, W., and R. A. Treumann (2001), *Advanced Space Plasma Physics*, 47 pp., rev. ed., Imperial Coll. Press, London.

Cairns, R. A. (1979), The role of negative energy waves in some instabilities of parallel flows, *J. Fluid. Mech.*, *92*, 1–14.

Chandrasekhar, S. (1961), *Hydrodynamic and Hydromagnetic Stability*, pp. 481–514, Oxford Univ. Press, Oxford, U. K.

Chen, S.-H., and A. Hasegawa (1993), A theory of long-period magnetic pulsations: 1. Steady state excitation of field line resonances, *J. Geophys. Res.*, *79*(7), 1024–1032.

Chen, S.-H., and M. G. Kivelson (1993), On non-sinusoidal waves at the magnetopause, *Geophys. Res. Lett.*, *20*, 2699–2702.

Fairfield, D. H., A. Otto, S. Kokobun, R. P. Lepping, J. T. Steinberg, A. J. Lazarus, and T. Yamamoto (2000), Geotail observation of Kelvin-Helmholtz at the equatorial magnetotail boundary for parallel northward fields, *J. Geophys. Res.*, *105*(A9), 21,159–21,173.

Fejer, J. A. (1963), Hydromagnetic reflection and refraction at a fluid velocity discontinuity, *Phys. Fluids*, *6*, 508–512.

Fejer, J. A. (1964), Hydromagnetic stability at a fluid velocity discontinuity between compressible fluids, *Phys. Fluids*, *7*, 499–503.

Foullon, C., C. J. Farrugia, A. N. Fazakerley, C. J. Owen, F. T. Gratton, and R. B. Torbert (2008), Evolution of Kelvin-Helmholtz activity on the dusk flank magnetopause, *J. Geophys. Res.*, *113*, A11203, doi:10.1029/2008JA013175.

Foullon, C., C. J. Farrugia, C. J. Owen, A. N. Fazakerley, and F. R. Gratton (2010), Kelvin-Helmholtz multi-spacecraft at the Earth's magnetopause boundaries, *AIP Conf. Proc.*, *1216,* 483, doi:10.1063/1.3395908.

Fujita, S., K.-H. Galssmeier, and K. Kamide (1996), MHD waves generated by the Kelvin-Helmholtz instability in a nonuniform magnetosphere, *J. Geophys. Res.*, *101*, 27,317–27,325.

Gnavi, G., F. T. Gratton, C. J. Farrugia, and L. E. Bilbao (2009), Supersonic mixing layers: Stability of magnetospheric flanks models, *J. Phys. Conf. Ser.*, *166*, 1–15, doi:10.1088/1742-6596/166/1/012022.

González, A. G., and J. Gratton (1994), The role of a density jump in the Kelvin-Helmholtz instability of a compressible plasma, *J. Plasma Phys.*, *52*(2), 223–244.

González, A. G., J. Gratton, F. T. Gratton, and C. J. Farrugia (2002), Compressible Kelvin-Helmholtz instability at the terrestrial magnetopause, *Braz. J. of Phys.*, *32*(4), 945–963.

Hasegawa, H., M. Fujitomo, T.-D. Phan, H. Réme, H. Balogh, M. W. Dunlop, C. Hashimoto, and R. TanDokoro (2004), Transport of solar wind into Earth's magnetosphere through rolled-up Kelvin-Helmholtz vortices, *Lett. Nat.*, *430*, 755–758, doi:10.1038/nature02799.

Hasegawa, H., M. Fujitomo, K. Takagi, Y. Saito, and H. Réme (2006), Single-spacecraft detection of rolled-up Kelvin-Helmholtz vortices at the flank magnetopause, *J. Geophys. Res.*, *111*, A09203, doi:10.1029/2006JA011728.

Hwang, K.-J., M. M. Kuznetsova, F. Sahraoui, M. L. Goldstein, E. Lee, and G. K. Parks (2011), Kelvin-Helmholtz waves under southward IMF, *J. Geophys. Res.*, *116*, A08210, doi:10.1029/2011JA016596.

Itoh, K., H. Nakamura, H. Kumamaru, and Y. Kukita (2004), Internal-shear mode instabilities on high-speed liquid jet, (I) characteristics of linear solutions, *J. Nucl. Sci. Technol.*, *41*(8), 802–808.

Kato, Y., M. Tajiri, and T. Taniuti (1966), Propagation of hydromagnetic waves in collisionless plasma. 1, *J. Phys. Soc. Jpn.*, *21*(4), 765–777.

Kivelson, M. G., and S.-H. Chen (1995), The magnetopause: Surface waves and instabilities and their possible dynamical consequences, in *Physics of the Magnetopause, Geophys. Monogr. Ser.,* vol. 90, edited by P. Song, B. U. Sonnerup, and M. F. Thomsen, pp. 257–268, AGU, Washington, D. C., doi:10.1029/GM090p0257.

Lavraud, B. J, and E. Borovsky (2008), *J. Geophys. Res.*, *113*, A00B08, doi:10.1029/2008JA013192.

Lavraud, B., J. E. Borovsky, A. J. Ridley, E. W. Pogue, M. F. Thomsen, A. N. Réme, A. N. Fazakerley, and E. A. Lucek (2007), Strong bulk plasma acceleration in earth's magnetosheath: A magnetic slingshot effect? *Geop. Res. Lett.*, *34*, L14102, doi:10.1029/2007GL030024.

Lerche, I. (1966), Validity of hydromagnetic approach in discussing instability of the magnetospheric boundary, *J. Geophys. Res.*, *71*(9), 2365–2371.

Lui, A. T. Y. (2004), Potential plasma instabilities for the substorm expansion onset, *Space Sci. Rev.*, *113*, 127–206.

Mann, I. R., A. N. Wright, K. J. Mills, and V. M. Nakariakov (1999), Excitation of magnetospheric waveguide modes by magnetosheath flows, *J. Geophys. Res.*, *104*(A1), 333–353.

McKenzie, J. F. (1970), Hydromagnetic wave interaction with the magnetopause and the bow shock, *J. Geophys. Res.*, *18*, 1–23.

Mills, K. J., and A. N. Wright (1999), Azimuthal phase speeds of field line resonances driven by Kelvin-Helmholtz unstable waveguide modes, *J. Geophys. Res.*, *104*(A10), 22,667–22,677.

Mills, K. J., A. N. Wright, and I. R. Mann (1999), Kelvin-Helmholtz driven modes of the magnetosphere, *Phys. Plasmas*, *6*(10), 4070–4087.

Miura, A. (1984), Anamolous transport by magnetohydrodynamic Kelvin-Helmholtz instabilities in the solar wind-magnetosphere interactions, *J. Geophys. Res.*, *89*(A2), 801–818.

Miura, A. (1995), Dependence of the magnetopause Kelvin-Helmholtz instability on the orientation of the magnetosheath field, *Geophys. Res. Lett.*, *22*(21), 2993–2996.

Miura, A., and P. L. Pritchett (1982), Nonlocal stability analysis of the MHD Kelvin-Helmholtz instability in a compressible plasma, *J. Geophys. Res.*, *87*(A9), 7431–7444.

Nakai, H., and G. Ueno (2011), Plasma structures of Kelvin-Helmholtz billows at the dusk-side flank of the magnetotail, *J. Geophys. Res.*, *116*, A08212, doi:10.1029/2010JA0116286.

Nakamura, T. K. M., M. Fujitomo, and A. Otto (2006), Magnetic reconnection induced by Kelvin-Helmholtz instability and the formation of the low-latitude boundary layer, *Geophys. Res. Lett.*, *33*, L14106, doi:10.1029/2006GL026318.

Namikawa, T., and H. Hamabata (1981), Propagation of the hydromagnetic waves through a collisionless heat-conducting plasma, *J. Plasma Phys.*, *26*, 95–121.

Ong, R. S. B., and N. Roderick (1972), On the Kelvin-Helmholtz instability of the Earth's magnetopause, *Planet. Space Sci.*, *20*, 1–10.

Otto, A., and D. H Fairfield (2000), *J. Geophys. Res.*, *105*(A9), 21,175–21,190.

Owen, C. J., M. G. G. T. Taylor, I. C. Krauklis, A. N. Fazakerley, M. W. Dunlop, and J. M. Bosqued (2004), Cluster observations of surface waves on the dawn flank magnetopause, *Ann. Geophys.*, *22*, 971–983.

Pegoraro, F., M. Faganello, and F. Califano (2008), Collisionless Kelvin-Helmholtz instability and vortex-induced reconnection in the external region of the earth magnetotail, *J. Phys. Conf. Ser.*, *133*, 012024, doi:10.1088/1742-6596/133/1/012024.

Pertinec, S. M., and C. T. Russell (1996), Near-earth magnetotail shape and size as determined from the magnetopause flaring angle, *J. Geophys. Res.*, *101*(A1), 137–152.

Pu, Z.-Y., and M. G. Kivelson (1983a), Kelvin-Helmholtz instability at the magnetopause: Solution for compressible plasmas, *J. Geophys. Res.*, *88*(A2), 841–852.

Pu, Z.-Y., and M. G. Kivelson (1983b), Kelvin-Helmholtz instability at the magnetopause: Energy flux into the magnetosphere, *J. Geophys. Res.*, *88* (A2), 853–861.

Rae, I. J., et al. (2005), Evolution and characteristics of global Pc5 ULF waves during a high solar wind speed, *J. Geophys. Res.*, *110*, A12211, doi:10.1029/2005JA011007.

Rostoker, G., and T. Eastman (1987), A boundary layer model for magnetospheric substorms, *J. Geophys. Res.*, *92*, 12,187–12,201.

Sen, A. K. (1963), Stability of hydromagnetic Kelvin-Helmholtz discontinuity, *Phys. Fluids*, *6*, 1154–1163.

Sen, A. K. (1964), Effect of compressibility on Kelvin-Helmholtz instability in a plasma, *Phys. Fluids*, *216*, 1293–1298.

Sen, A. K. (1965), Stability of magnetospheric boundary, *Planet. Space Sci.*, *13*, 131–141.

Shiryeava, S. O. (2001), Linear wave interaction at the charged fluid-fluid interface under tangential discontinuity of the velocity field, *Tech. Phys.*, *46*, 280–286.

Southwood, D. J. (1968), The hydromagnetic stability of the magnetospheric boundary, *Planet. Space Sci.*, *16*, 587–605.

Southwood, D. J. (1974), Some features of field line resonances in the magnetosphere, *Planet. Space Sci.*, *22*, 483–491.

Swanson, D. G. (1989), *Plasma Waves*, 2nd ed., 239 pp., Academic, Boston, Mass.

Tajiri, M. (1967), Propagation of hydromagnetic waves in collisionless plasma. 2, kinetic approach, *J. Phys. Soc. Jpn.*, *22*(6), 1482–1494.

Taroyan, Y., and R. Erdélyi (2002), Resonant and Kelvin-Helmholtz instabilities on the magnetopause, *Phys. Plasmas*, *9*(7), 3121–3129.

Taroyan, Y., and R. Erdélyi (2003a), Resonant surface waves and instabilities in finite β plasmas, *Phys. Plasmas*, *10*(1), 266–276.

Taroyan, Y., and R. Erdélyi (2003b), On resonantly excited MHD waves in the magnetotail, *J. Geophys. Res.*, *108*(A1), 1043, doi:10.1029/2002JA009586.

Uberoi, C. (2006), Surface waves induced magnetic reconnection and quantification of space weather phenomena, ILWS Workshop.

Villante, U. (2007), Ultra low frequency waves in the magnetosphere, in *Handbook of the Solar-Terrestrial Environment*, edited by Y. Kamide and Y. Chian, pp. 397–422, Springer, Berlin.

Walker, A. D. M. (1981), Kelvin-Helmholtz instability in the low-latitude boundary layer, *Planet. Space Sci.*, *29*(10), 1119–1133.

Walker, A. D. M (2000), Reflection and transmission at the boundary between two counter-streaming MHD plasmas-active boundaries or negative-energy waves, *J. Geophys. Res.*, *3*(63), 203–219.

Yoon, P.-H., J. F. Darake, and A. T. Y. Lui (1996), Theory and simulation of Kelvin-Helmholtz instability in the geomagnetic tail, *J. Geophys. Res.*, *101*, 27,327–27,339.